

Invited paper

Effect of Ti—F surface interaction on the photocatalytic degradation of phenol, aniline and formic acid

W. El-Alami^{a,b,c}, D. Garzón Sousa^{b,c,*}, C. Fernández Rodríguez^{b,c}, O. González Díaz^{b,c}, J.M. Doña Rodríguez^{b,c}, M. El Azzouzi^a, J. Araña^{b,c,*}^a Faculté des Sciences, Université Mohammed V, Agdal, BP 1014 Avenue Ibn Batoutta, Rabat, Morocco^b CIDIA-FEAM Universidad de La Palmas de Gran Canaria, Edificio del Parque Científico Tecnológico de la ULPGC, Campus de Tafira, 35017 La Palmas de Gran Canaria, (Unidad Asociada al CSIC a través del Instituto de Ciencias de Materiales de Sevilla, ICMS), Spain^c Instituto de Estudios Ambientales y Recursos Naturales (i-UNAT)-ULPGC, Spain

ARTICLE INFO

Article history:

Received 27 April 2017

Received in revised form 27 July 2017

Accepted 7 August 2017

Available online 22 August 2017

Keywords:

F-TiO₂

FTIR

Phenol

Aniline

Formic acid

ABSTRACT

A study is undertaken of the effect of fluorinating two TiO₂ catalysts, both with the same surface area but one composed only of pure anatase phase (SA) and the other of mixed anatase and rutile phases (P25), on the degradation of phenol, formic acid and aniline. The catalysts were characterised by FTIR, BET, EDAXs, SEM, XRD and DRS-UV-vis studies. The method used for synthesis of the F-P25 and F-SA resulted in fluorinated catalysts with properties different to those of other fluorinated catalysts reported in the bibliography. The results obtained show that, unlike other studies in which the formation of free hydroxyl radicals ($\cdot\text{OH}_{\text{free}}$) was enhanced with the fluorinated catalysts, in the F-P25 and F-SA catalysts it was the formation of surface hydroxyl radicals ($\cdot\text{OH}_{\text{surf}}$) which was significantly enhanced. In this way, the F-P25 and F-SA catalysts gave rise to higher degradation rate constants of phenol (k_{phenol}), aniline (k_{aniline}) and formic acid (k_{formic}) than the P25 and SA catalysts.

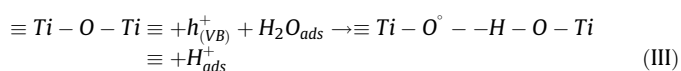
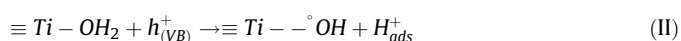
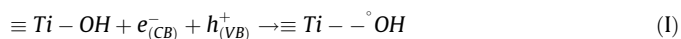
© 2017 Elsevier B.V. All rights reserved.

1. Introduction

The capacity of TiO₂ to degrade organic compounds has been demonstrated in numerous studies. However, the efficiency of this semiconductor needs to be improved for it to be an effective tool for pollutant removal. Various processes have been developed with the aim of enhancing and optimizing its photocatalytic properties. Fluoride has been used as precursor to synthesise new catalysts in which the exposure of certain crystalline faces is increased [1–5]. Research has also been conducted on surface modification of TiO₂ with fluorine (F-TiO₂). Fluorine has a higher electronegativity than oxygen and a specific affinity for adsorption onto TiO₂ acting as a Lewis base. The presence of fluoride anions has shown positive effects in aqueous phase increasing the degradation rate of phenol

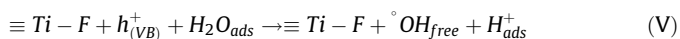
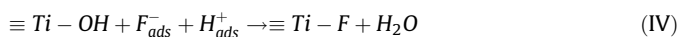
[6], benzoic acid [7], cyanuric acid (Triazine-2, 4, 6-Triol) [8], benzene, 4-chlorophenol [9], as well as several dyes [10,11].

Different studies have shown that TiO₂ fluorination does not change the band gap of this semiconductor as the *p* orbitals of the fluorine have a lower energy than those of the oxygen atoms [12–14]. It has also been shown that the strong electron acceptor capacity of the Ti—F groups present on the surface hinders recombination of photo-generated electrons and holes, thereby enhancing photocatalytic efficiency [12–15]. It has been reported that the increased degradation rate is due to the increase in the concentration of $\cdot\text{OH}$ radicals in solution as the fluorides displace the $\cdot\text{OH}$ groups from the surface [6]. In this respect, the following mechanisms have been proposed [6]:



* Corresponding authors at: CIDIA-FEAM Universidad de La Palmas de Gran Canaria, Edificio del Parque Científico Tecnológico de la ULPGC, Campus de Tafira, 35017 La Palmas de Gran Canaria, (Unidad Asociada al CSIC a través del Instituto de Ciencias de Materiales de Sevilla, ICMS), Spain.

E-mail addresses: d.garzon.sousa@gmail.com (D. G. Sousa), javier.arana@ulpgc.es (J. Araña).



However, the physical chemistry of this process as well as many other aspects of the effect of fluorine on the TiO_2 surface have not been fully clarified [15].

It has been reported that the doping of anatase TiO_2 with elements like F with extra electrons gives rise to *n*-type materials with significantly different properties to those of the original catalyst [16]. The extra electrons provided by the F^- ions are stabilised on the titanium ions of the crystal lattice giving rise to Ti^{3+} ions homogeneously spread over the crystal lattice. Titanium dioxide is a reducible oxide whose composition depends, among other factors, on oxygen pressure in the atmosphere. The extra electron provided by the fluorine will be found in the Ti 3d orbitals a few tenths of an electron-volt below the lower end of the conduction band [17]. TiO_2 doping with fluorine gives rise to two types of fluoride species. The first of these arises when the F^- ion replaces the O^{2-} ions of the crystal lattice resulting in $\text{Ti}-\text{F}-\text{Ti}$ bonds. This leads to the formation of Ti^{3+} species in the bulk, giving rise to localised Ti^{3+} states just below the conduction band. This type of doping inhibits oxygen adsorption and consequently the formation of superoxide radicals, suggesting that the sites with defects are localised in the bulk and not on the surface. The second species consists of F^- ions on the surface of the solid which replace surface hydroxyl groups giving rise to $\text{Ti}-\text{F}$ terminal groups without generating reduced sites [17]. The Ti^{3+} sites that are generated may be systems entirely localised in sections of the catalyst or systems in which there is a total delocalisation of electron density in all the ions of the metal, with the energy levels of these states just below the conduction band [16]. Studies undertaken to date suggest that the second of these possibilities appears to be the most probable [18]. Displacement of the negative charge, which takes place at the edges of the energy levels, favours the charge transference rate and lowers the recombination rate. The accumulation of electrons trapped in the conduction band in a photo-stationary state results in the surface charge of the TiO_2 suspended particles changing to negative [19]. Most of the electrons would be localised on $\text{Ti}(\text{III})-\text{OH}$ surface sites.

It has been reported in other studies that an increase in the degradation rate takes place when the anatase phase is doped with fluorine, but that this rate decreases when the rutile phase of the TiO_2 is doped [20]. It was also shown in the same study that the increase in the degradation rate does not always require pre-adsorption of the fluoride ions. A Helmholtz double layer was proposed by the authors of the study in which the fluoride ions would be situated on the internal and external planes of this double layer, facilitating desorption of the surface bonded ${}^\circ\text{OH}$ radicals to the solution upon irradiation of the TiO_2 . The most active radical fluorides are those found in the outer Helmholtz layer, and are the most efficient at provoking desorption of the surface bonded ${}^\circ\text{OH}$ radicals. The inner layer fluoride ions, namely those adsorbed onto the surface or bonded to Ti^{4+} sites, have a lower capacity to form a bond with the surface bonded ${}^\circ\text{OH}$ via hydrogen-fluorine bridges. The key to this proposal lies in the argument that desorption to the solution of the surface bonded hydroxyl radicals on the irradiated TiO_2 is thermodynamically possible through an $\text{H}-\text{F}$ bond [20].

It should also be noted that a positive effect has not been observed in all studies involving TiO_2 doping with fluorine. For example, a slowing down of the degradation rate of dichloroacetate [21] and of the degradation rate in gas phase of some

compounds [22] has been observed. As previously stated, the fluoride ion has a specific affinity for adsorption on TiO_2 acting as a Lewis base, and so would decrease and modify the density of surface states and, in this way, slow down certain degradation processes [15]. It should also be noted that although the formation of ${}^\circ\text{OH}$ radicals is higher in F-TiO_2 , the oxidation processes in which there is hole transfer are inhibited [21].

In order to acquire a more in-depth knowledge and understanding of the behaviour of these fluorinated materials, a study is undertaken in the present work of the degradation of phenol, formic acid and aniline with two TiO_2 catalysts with different anatase and rutile phase proportions. For this purpose, the P25 catalyst with 80% anatase and 20% rutile phase and the Sigma Aldrich (SA) catalyst with purely anatase phase were selected. Both materials have approximately the same surface area (about $50\text{ m}^2\text{ g}^{-1}$). These two catalysts were fluorinated using high concentrations of NaF at pH 6.5 and selecting the filtration method to obtain the corresponding F-P25 and F-SA catalysts.

Various organic compounds have been described in the bibliography to assess the photocatalytic activity of materials with different physical-chemical properties. These include coumarin, terephthalic acid, phenol, aniline and/or formic acid, depending principally, among other aspects, on determining what type of radical intervenes or whether adsorption is a determinant factor in the process [23,24]. Considering the working pH values, the degradation mechanisms and the results described in the bibliography, formic acid, aniline and phenol were selected in the present work as test molecules to characterise the catalysts.

2. Experimental

2.1. Synthesis of fluorinated catalysts

Two commercial TiO_2 photocatalysts were used: Evonik Aeroxide P25 (P25) and anatase Sigma Aldrich (SA). For the synthesis of the fluorinated catalysts, 10 g of the corresponding commercial TiO_2 catalyst were placed into 250 mL of a 2 M NaF solution (pH 6.5). This solution was stirred continuously for 30 min and then filtered. The catalyst obtained after filtration was washed with 1 L of water and the non-desorption of fluoride and sodium was observed. The catalyst was subsequently dried at 100°C for 12 h. It should be noted that different filters were tested with different pore diameters and that important photocatalytic performances were only obtained with the Whatman TM 1005-125 (grade 5, diameter: 12.5 cm, pore size: $2.5\text{ }\mu\text{m}$).

2.2. Characterisation of materials

The surface concentration of fluorine on the catalysts was semi-quantitatively determined by EDAX analysis (Quantax 70, Bruker). Three image amplifications were carried out for this analysis (300, 3000 and 30,000) with 5 sampling points in each increase and an exposure time of 300 s.

Analyses of the crystalline structure were performed by X-ray diffraction (XRD Bruker D8 Advance) with a source of $\text{Cu K}\alpha_1$ radiation ($\lambda = 0.15406\text{ nm}$) at 1.6 kW (40 kV, 40 mA). Anatase-rutile fractions were calculated taking into account the relative diffraction peak intensities of crystalline planes (101) and (111) of anatase and rutile, respectively. BET surface area measurements were carried out by N_2 adsorption at 77 K using a Micromeritics 2010 instrument. Diffuse reflectance UV-vis spectra (DRS-UV-vis) were recorded on a Varian Cary 5 spectrometer equipped with an integrating sphere using PTFE (poly-tetra-fluoroethylene) as reference to study the optoelectronic properties of the samples. Diffuse reflectance spectra were recorded and band gap values

were calculated by the Kubelka-Munk function, according to the Tandon-Gupta method. Field emission scanning electron microscopy (FESEM) images were obtained using a Hitachi S-4800 microscope.

The Brönsted and Lewis acid sites determination was done through interaction of ammonia with the surface of the catalysts. This interaction was followed by Fourier transform infrared spectroscopy (FTIR) with a Thermo-Scientific-Nicolet iS10 spectrophotometer and a custom-made cell equipped with CaF_2 windows performing 32 scans with a spectral resolution of 4 cm^{-1} . 10 mg of catalyst were used in each experiment. Catalysts were treated with a stream of saturated moist air with an NH_3 molar flow rate of $6.24 \cdot 10^{-4}\text{ mol min}^{-1}$ for 60 min and then placed in the cell for analysis. The system has been described in a previous work [25].

2.3. Photocatalytic experiments

The degradation tests were performed in 250 mL Pyrex glass batch reactors, filled with 200 mL of the pollutant aqueous solution and 1 g/L of P25, SA, F-P25 or F-SA. A constant stirring was maintained at 750 rpm. A 60W Philips Solarium HB175 equipped with four 15W Philips CLEO fluorescent tubes with emission spectrum from 300 to 400 nm (maximum around 365 nm) and with an average irradiation power of about 9 mW was used as UV source in the photocatalytic studies. The pH was adjusted with diluted H_2SO_4 or NaOH. Before irradiation was turned on, the solution was left for 15 min in the darkness to reach the adsorption-desorption quasi-equilibrium. Adsorption was lower than 5% after this period with all catalysts.

All the studies were performed with a 0.51 mM concentration of phenol, aniline or formic acid. The studies with formic acid were performed at pH 3, those with phenol at pH 5 and those with aniline at pH 7, with the aim of ensuring that the molecule under study had the appropriate electrical charge to facilitate its approximation to the photocatalyst surface. A constant pH was maintained throughout the test.

2.3.1. Analytical determinations

Concentrations of phenol, aniline and formic acid at different reaction times were HPLC-measured using a Supelco Discovery C18 ($25\text{ cm} \times 4.6\text{ mm ID}$, $5\text{ }\mu\text{m}$ particles) for phenol and aniline and a Supelcogel C-610H ($30\text{ cm} \times 7.8\text{ mm ID}$) for formic acid. The mobile phase used were acetonitrile-water-acetic acid (30:69:5:0.5% vol) for phenol, acetonitrile- acetate buffer 0.01 M (30:70) for aniline and phosphoric acid-water (0.1:99.9) for formic acid. Detector wavelength was 270 nm for phenol and 230 nm for aniline and formic acid. Quantification was performed by least-squares fit.

The concentrations of phenol and muconic acid in the studies performed with mixtures of these compounds were made using an EC 250/4 Nucleodur 100-5 C18ec column ($250\text{ mm} \times 4\text{ mm ID}$, $5\text{ }\mu\text{m}$ particles). The mobile phase used was acetonitrile/water/ H_3PO_4 15/85/0.1. Detector wavelength in these studies was 264 nm. Quantification was also performed by least-squares fit.

The total organic carbon (TOC) analyses were determined using an analyser (TOC-VCSN, Shimadzu).

3. Results and discussion

3.1. BET area, EDAX, SEM, XRD and DRS-UV-vis analyses

Table 1 shows the most important results of the BET, EDAX, DRX and DRS-UV-vis analyses. P25 and SA catalysts have respective surface areas of 50.9 and $47.3\text{ m}^2\text{ g}^{-1}$. The fluorinated catalysts, F-P25 and F-SA, have similar surface areas (51.3 and $45.4\text{ m}^2/\text{g}$ respectively). The anatase/rutile phase ratios of the P25 and F-P25 are 82.3/17.7 and 85.5/14.5 respectively, while the SA and F-SA catalysts only have anatase phase. The mean particle size was also determined; it was noted that they were very similar in the P25 and F-P25, but that there was a difference in size of approximately 7 nm between the anatase particles of the SA and F-SA. The differences observed are attributable to the filtration process of the catalyst in the synthesis of the fluorinated materials. The band gap values obtained from the UV-vis analyses are all very similar, with no significant changes observed when fluorinating the catalysts. Thus, as seen in other studies, surface fluorination of the catalysts does not modify the optical properties of these materials [26,27]. The images obtained from the SEM analyses of the F-P25, F-SA and SA catalysts show a similar distribution of aggregates (Fig. 1). However SEM analyses of the P25 show a different distribution of aggregates, which can also be attributed to the filtration process.

Table 1 also shows the Ti/F and F/Na ratios obtained from the EDAX analyses. The analyses also showed the presence of sodium on the surface of the fluorinated materials, though its concentration is significantly lower than the molar concentration of fluorine. This shows that the fluorine is mostly interacting with the catalyst surface and is not as NaF, though the presence of this salt on the surface cannot be discarded. Note that the Ti/F proportions in both fluorinated catalysts are similar.

3.2. Characterisation of the adsorbed water, hydroxyl groups and surface charge

Fig. 2 shows the spectra of the fluorinated and non-fluorinated P25 and SA catalysts. Note in particular the position of the baseline in each of these catalysts, the band attributed to isolated hydroxyl groups (3698 cm^{-1}) and the bands attributed to adsorbed water ($3600\text{--}3000\text{ cm}^{-1}$ and 1640 cm^{-1}).

An important feature to note in the spectra of Fig. 2 is the position of the baseline. As a result of the presence of surface or shallow electron traps, electrons are fed to the conduction band via thermal processes such as those generated by the infrared radiation used to obtain the spectra. The electrons promoted to the conduction band have a similar behaviour to that described for delocalised electrons confined to a three-dimensional box with infinite walls; the high density of generated states gives rise to the continuous presence of excited electrons leading to a baseline increase of the infrared spectrum [16]. The baseline position of the

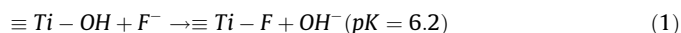
Table 1
Surface area, anatase/rutile phase ratios, crystallite size, band gap and Ti/F and F/Na molar ratios.

	Surface area ($\text{m}^2\text{ g}^{-1}$)	Anatase/rutile phase ratios	Crystallite size (nm)		Band gap (eV)	Molar ratio	
			Anatase	Rutile		Ti/F	F/Na
P25	50.9	82.3/17.7	20.56	33.01	3.16	–	–
F-P25	51.3	85.5/14.5	19.84	34.70	3.0	20.97	2.47
SA	47.3	100/0	13.93	–	3.16	–	–
F-SA	45.4	100/0	20.57	–	3.18	19.43	2.12

Fig. 1. Imagen SEM of the fluorinated and non-fluorinated P25 and SA catalysts.

baseline increase observed in the F-P25 catalysts [17]. Modification of the baseline also takes place with the F-SA catalyst in the region between 2500 and 1000 cm^{-1} as a consequence of the presence of fluoride.

The fluorination process has been described through Reaction (1) [4].



Bearing in mind the pK of Reaction (1), the highest percentage of fluorination is produced around pH 3 [28,29]. However, in the present work, impregnation with NaF was performed at pH 6.5, and so in the spectra of the fluorinated catalysts (Fig. 2) bands of isolated hydroxyl groups (3698 cm^{-1}) are still observed and in an even relatively higher proportion than with the P25 and SA catalysts.

Fig. 2. FTIR spectra of the fluorinated and non-fluorinated P25 and SA catalysts.

SA catalyst, the one with only anatase phase, is higher than that of the P25. On modification of P25 with fluorine, a baseline increase takes place which takes it to the same level as that observed in the SA catalyst. When TiO_2 is modified with fluorine, at least a fraction of the excess electrons introduced by the fluorine are localised by lattice Ti^{4+} cations. The presence of reduced Ti^{3+} centres in the as-prepared, fully oxidised solid indicates that the F- TiO_2 system can be described in terms of an *n*-type semiconductor provoking the

3.3. Determination of Lewis and Brönsted acid sites

Ammonia can interact with Brönsted and Lewis acidic surface sites forming ammonium ions and acid-base adducts, respectively. The presence of these species can be perfectly identified via FTIR. The interaction of NH_3 with the Lewis acid sites gives rise to bands centred around 1200 cm^{-1} ; the higher the wavenumber the greater the strength of the Lewis sites. The non-adsorbed NH_4^+ gives rise to a band centred around 1445 cm^{-1} , and the shift of this band to higher wavenumbers would indicate the presence of adsorbed ammonium.

The spectra obtained from the interaction of ammonia with the catalysts are shown in Fig. 3. A broad band centred around 1200 cm^{-1} can be observed in the initial spectrum of the P25 attributed to $\delta_s\text{NH}_3$ ammonia adsorbed on Lewis sites. The asymmetry and width of the band suggest that it may be composed of Lewis acid sites of different types. A broad band can also be observed at 1445 cm^{-1} which is attributed to the $\delta_{\text{as}}\text{NH}_4^+$ vibration. The width of this band may be due to its being formed of free ammonium produced by the abstraction of a proton from the P25 surface present in a Brönsted acid site and adsorbed ammonia [30,31]. A further band can be observed at 1315 cm^{-1} and a shoulder at 1558 cm^{-1} which cannot be attributed to ammonia adsorbed on either Lewis or Brönsted acid sites. It has been suggested in some studies that these bands most likely represent various deformation vibrations of NH_x species, which are formed on the surface in relatively small amounts as a result of NH_3 adsorption [32].

In the spectrum obtained of the interaction of NH_3 with the SA catalyst, the band attributed to the $\delta_{\text{as}}\text{NH}_4^+$ vibration is found at the same wavenumber, 1445 cm^{-1} , as in the P25 studies. However, the band attributed to the Lewis acid sites is found at 1216 cm^{-1} and the band corresponding to compounds generated by the decomposition of the ammonia has low intensity.

In the spectrum of NH_3 interaction with the F-P25 and F-SA catalysts (Fig. 2), the absence of the band attributed to NH_3 adsorbed on Lewis acid sites should be noted. However, in these catalysts the band attributed to $\delta_{\text{as}}\text{NH}_4^+$ (1445 cm^{-1}) was observed and a band at 1340 cm^{-1} .

The initial spectrum observed with F-TiO₂ can be explained as the interaction of NH_3 with surface fluorine through the following reaction [33,34].

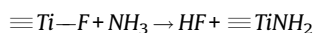


Fig. 3. FTIR spectra of the interaction of the NH_3 with the catalysts.

Fig. 4. Evolution of the concentration of formic acid during photocatalytic oxidation.

The non-detection of the band attributed to Lewis acid sites at around 1200 cm^{-1} in the fluorinated catalysts would suggest that in these materials the surface Ti atoms are fluorinated or strongly bonded to hydroxyl groups.

3.4. Photocatalytic degradation studies

As indicated in the experimental section, the formic acid, aniline and phenol degradation studies were all performed at the same concentration (0.51 mM). The pH of the solution in the different studies was 7, 5 and 3 for the aniline, phenol and formic acid, respectively.

Figs. 4–6 show the degradation results of formic acid, aniline and phenol, respectively. With all the substrates studied, the F-P25 catalyst showed the greatest photocatalytic efficiency in degradation. The F-SA and P25 had similar degradation curves for all the molecules, while the SA has the worst photocatalytic activity.

Fig. 7 shows the degradation constants for each catalyst and each substrate obtained from the results shown in Figs. 4–6. As can be observed, the rate constants display the following sequence with all the substrates:



With all catalysts, the highest rate constant is found with formic acid degradation, followed by phenol and with the slowest for

Fig. 5. Evolution of the concentration of aniline during photocatalytic oxidation.

Fig. 6. Evolution of the concentration of phenol during photocatalytic oxidation.

aniline. The rate constant with P25 in the formic acid degradation is 3.25 times greater than that of phenol, in the SA it is 2.15 times greater and in the fluorinated catalysts it is 1.5 times greater. Again with the P25, the degradation rate constant of phenol is, in turn, 1.8 times greater than that of aniline, whereas with the SA catalyst the rates are similar and in the fluorinated catalysts it is 3.7 times higher in the F-P25 and 2.5 times higher in the F-SA. The degradation sequence appears to be related to the oxidation state of the carbon in the compound. Thus, the more oxidised the substrate under study the faster the degradation.

To compare the efficiency of the fluorinated catalysts, the ratio between the rate constants of F-P25/P25 and of F-SA/SA with the different substrates was calculated (Fig. 8). The ratios obtained for phenol and aniline are practically the same for both catalysts. That is, for the phenol and aniline the same increase in the rate constant

Fig. 8. Ratio between apparent first order kinetic constants obtained for the fluorinated/bare catalysts (F-P25/P25 and F-SA/SA).

takes place when the catalysts are fluorinated. The highest increase in the rate constant is with the phenol. With the fluorinated P25 catalyst, the same increase in the rate constant is seen in aniline and formic acid degradation. However, with the SA catalyst a higher increase is observed in the degradation rate constant of formic acid than of aniline.

With a view to a greater in-depth study, tests were carried out with phenol in the presence of muconic acid with each at the same concentration of 0.51 mM (Fig. 9A), and at half that concentration (0.25 mM) (Fig. 9B). These studies were performed to see whether the presence of a phenol degradation intermediate (muconic acid) at high concentrations would vary the parameters determined in the previous studies. The rate constants obtained in these studies were compared with those of phenol alone, aniline and formic acid

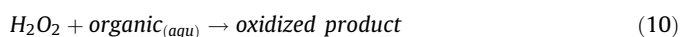
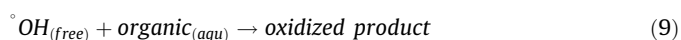
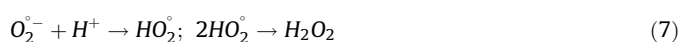
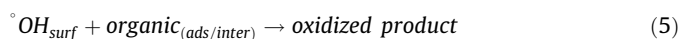
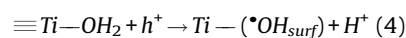
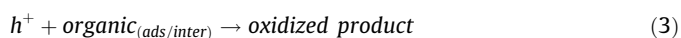
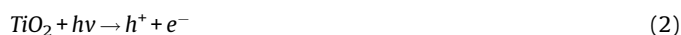
Fig. 7. Apparent first order kinetic constants for formic acid, aniline, phenol and muconic acid photocatalytic oxidation in presence of the different catalysts. Phenol-1: k_{phenol} in study with phenol 0.51 mM; Phenol-2: k_{phenol} in study with mixtures phenol:muconic acid (0.51 mM: 0.51 mM); Phenol-3: k_{phenol} in study with mixtures phenol:muconic acid (0.25 mM: 0.25 mM). Muconic-1: $k_{muconicacid}$ in study with muconic acid 0.51 mM; Muconic-2 $k_{muconicacid}$ in study with mixtures phenol:muconic acid (0.51 mM: 0.51 mM); Muconic-3: $k_{muconicacid}$ in study with mixtures phenol:muconic acid (0.25 mM: 0.25 mM); Muconic-4: $k_{muconicacid}$ in muconic acid photolysis.

A control was also performed of the main intermediates of phenol degradation (hydroquinone, catechol and resorcinol). Figs. 10 and 11 show the concentrations and evolution of these intermediates. In the studies with phenol alone, the concentrations of intermediates follow the sequence [resorcinol] ≥ [hydroquinone] > [catechol] with the all catalysts. With the F-P25, the concentrations of these intermediates decrease very rapidly. In the studies performed in the presence of muconic acid (0.51 mM), the concentrations of resorcinol are significantly smaller and the concentration of intermediates has the following sequence [hydroquinone] > [catechol] > [resorcinol].

A control was also performed of TOC. In order to evaluate the concentration of degradation intermediates other than dihydroxylated phenolic compounds, the concentrations of organic matter corresponding to phenol, hydroquinone, catechol, resorcinol and muconic acid determined in previous analyses (Fig. 12) were subtracted from the experimentally determined TOC. As can be seen, in all the studies the F-P25, which presents the highest k_{phenol} , has less capacity to mineralise the intermediates generated from the degradation of the dihydroxylated compounds.

3.5. Discussion of the results

The photocatalytic processes can be summarized in the following reactions [35]:



The oxidative species h^+ and $^{\bullet}OH_{surf}$ would give rise to oxidation processes on the catalyst surface or at the surface-solution (inter) interface, while the oxidative species $^{\bullet}OH_{(free)}$ and H_2O_2 would give rise to oxidation processes in the solution.

Different studies [16–19] have shown that, with the introduction of fluorine atoms on the TiO_2 surface and their interaction with the Ti surface atoms, states are generated with high negative charge density. This has been observed in the FTIR studies of the F-P25 and F-SA catalysts described in this paper. The presence of the surface states of high negative charge density means that during illumination the photogenerated holes are trapped on the surface and the electrons forced to make their way to more internal Ti atoms in the crystalline structure [36]. Thus, the holes can react

Fig. 9. Evolution of the concentration of phenol during photocatalytic oxidation of mixtures phenol:muconic acid 0.51 mM:0.51 mM (A) and 0.25 mM:0.25 mM (B).

(Fig. 7). Also shown in Fig. 7 are the degradation rate constants of the muconic acid alone (0.51 mM) and the phenol-muconic acid mixtures. The $k_{phenol-2}$ in the studies performed with phenol-muconic acid mixtures (0.5 mM–0.5 mM) decrease by almost half with all the catalysts compared to the $k_{phenol-1}$ (studies with 0.51 mM phenol alone) (Fig. 7). In contrast, the $k_{phenol-3}$ values obtained in the studies performed with 0.25 mM–0.25 mM phenol-muconic acid mixtures are similar to the $k_{phenol-1}$ values. The same thing was observed in the degradation rate constants of the muconic acid (Fig. 7). Given that phenol is barely adsorbed onto the catalyst [35], this could be indicating competition for the generated radicals. It was also observed in these tests that the phenol degradation rate constant follows the same sequence as in the previous studies. That is, the highest rate constant is obtained with the F-P25, followed by the F-SA which has a similar rate constant to the P25, and finally the SA. The correlation between the F-P25/P25 and F-SA/SA phenol degradation rate constants was also calculated (Fig. 8), with very similar degradation rate constant increases being obtained after fluorination as in the previous studies. On the other hand, no increase was observed in the muconic acid degradation rate constant with the fluorinated catalysts. In fact, there even appears a slight decrease in the value when the catalysts are fluorinated.

with the surface oxygen atoms and/or the adsorbed water favouring Reactions (3)–(5) or generating new $\bullet\text{OH}_{\text{free}}$ radicals via Reaction (11) [15].



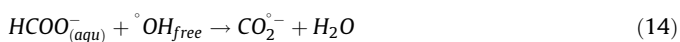
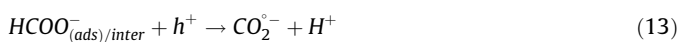
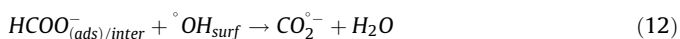
Depending on the reaction conditions, the reagents used and the reaction mechanism, the formation and/or intervention of these radicals can be favoured. The mechanisms described for the

lower than in anatase), a greater separation is favoured of the e^-/h^+ pair as a transfer of the holes is produced from the anatase to the rutile phase [41]. This would favour Reactions (3)–(10) in the P25 with respect to the SA. In the fluorinated catalysts, an increase was observed in the rate constant of 1.8 times in the F-P25 with respect to the P25 and of 3.13 times in the F-SA with respect to the SA. As previously indicated, when fluorinating the catalysts Reactions (3), (5) and/or (11) can be favoured.

degradation of formic acid, aniline and phenol are outlined in Diagrams 1–3 [37–39].

Degradation of formic acid can take place via reaction of the adsorbed (ads) formic acid or of the formic acid present at the solution/surface interface of the catalysts (inter) with the surface hydroxyl radicals ($\bullet\text{OH}_{\text{surf}}$) or holes (Reactions (12) and (13), respectively) or via the reaction of the formic acid in solution with free hydroxyl radicals ($\bullet\text{OH}_{\text{free}}$) (Reaction (14)).

Formic mechanism



In the formic acid degradation studies described in previous sections, it was observed that the rate constant was 3.5 times higher in the P25 than in the SA. The P25 is characterised as having anatase and rutile phases. It has been reported that the faces of the anatase phase have different conduction potential energy [40]. The electrons and holes generated migrate to different faces depending on their potential energy allowing, in this way, their separation. In fact, it has also been reported that there are preferential faces of the anatase phase for photooxidation processes and preferential faces for photoreduction [40]. However, in catalysts like the P25 in which anatase and rutile phases coexist, it has been reported that, due to the low diffusivity of electrons in the rutile phase (89 times

The degradation mechanisms of aniline and phenol, at the working pH values, are described in Diagrams 2 and 3.

In the phenol degradation mechanism, depending on the intermediate generated, it can be determined which reaction is favoured between (3), (5) and (9) or (11). It has thus been reported that resorcinol is generated from the reaction of phenol directly with the holes (Reaction (3)), hydroquinone from its reaction with the $\bullet\text{OH}_{\text{surf}}$ (Reaction (5)) and catechol from its reaction with the $\bullet\text{OH}_{\text{free}}$ (Reaction (9) or (11)) [35]. In other studies performed with fluorinated catalysts on phenol degradation, in addition to an increase in the phenol degradation rate constant (in the fluorinated catalysts), a significant increase was also observed in catechol concentrations with respect to hydroquinone concentrations [6,20,42,43]. This has been attributed to Reaction (11) being favoured in these catalysts. However, in the different phenol degradation studies in the present work (with and without muconic acid) performed with the F-P25 and F-SA catalysts, although there was an increase of between 3.6 and 4 times in the phenol degradation rate constant, in no test was there observed a higher concentration of catechol than of hydroquinone. This would suggest that Reaction (11) is not taking place in the studies performed with phenol with the F-P25 and F-SA catalysts. In these catalysts, the reactions which appear to be taking place are (3) and (5), with Reaction (9) taking place to a lesser degree. That is, in these catalysts it seems that what is influential are the electrostatic effects that decrease the reaction rate of the e^-/h^+ pair and which in this way promote reaction with the $\bullet\text{OH}_{\text{surf}}$ (Reaction (5)) or with the holes (Reaction (3)). In fact, in the characterisation studies the presence was observed of isolated hydroxyl groups in an even higher proportion than in the P25 and SA, as well as Brönsted acid sites.

Fig. 10. Evolution of intermediates catechol, hydroquinone and resorcinol during phenol degradation (A), mixtures phenol: muconic acid 0.51 mM:0.51 mM (B) and mixtures phenol: muconic acid 0.25 mM:0.25 mM (C) with P25 and F-P25.

In the phenol degradation studies in the presence of 0.5 mM muconic acid concentrations, it was observed that the phenol degradation rate constant was reduced practically by half in all the catalysts compared to the studies without this acid. Also reduced by half was the k_{muconic} compared to that of the studies without the presence of phenol. It was observed in the analysis of the intermediates that in the studies with muconic acid the concentrations of resorcinol were drastically reduced. This would suggest

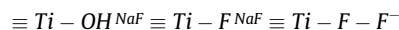
Fig. 11. Evolution of intermediates catechol, hydroquinone and resorcinol during phenol degradation (A), mixtures phenol: muconic acid 0.51 mM:0.51 mM (B) and mixtures phenol: muconic acid 0.25 mM:0.25 mM (C) with SA and F-SA.

that Reaction (3) of phenol with the holes would be inhibited in the presence of muconic acid. Muconic acid can be degraded by direct reaction of carboxylic acids with the holes (Kolbe reaction) or by means of the attack of $\cdot\text{OH}$ radicals on olefinic groups. The fact that the concentration of resorcinol decreases in these conditions and

but does have access to the $\bullet\text{OH}_{\text{surf}}$, in this way partially inhibiting muconic acid degradation. For this reason, the rate constants of both are reduced by half. Meanwhile, the k_{muconic} with the fluorinated catalysts is in all cases lower than that of the P25 and SA. This may be due to electrostatic repulsions which partially inhibit access to the surface of the fluorinated catalysts in the ionized form of this acid and to a significant number of Ti surface atoms being bonded to the fluorine (Table 1). The muconic acid at the study pH is principally in ionized form. However, the phenol and aniline are, at the study pH, in a suitable molecular form to be at the surface/solution interface.

As previously mentioned, in the three studies performed with phenol and in the study performed with aniline, approximately the same increase was observed in the k_{phenol} of the F-P25 and F-SA with respect to the P25 and SA, respectively (Fig. 8). That is, although the P25 has a higher k_{phenol} than the SA, when fluorinating both catalysts there takes place practically the same increase in the rate constant. This would suggest that in the fluorination process performed in this study the photoactive sites are being promoted in the same proportion.

The differences in the fluorination process carried out in this work compared to those carried out in other studies are that a much higher NaF concentration was used in this study and a specific type of aggregate was selected via filtration. Under these conditions, it has been reported in the bibliography that the process that takes place is [29]:



Therefore, in the F-P25 and F-SA the typical Ti–F centres that give rise to Reaction (11) do not appear, but the electrostatic effect is produced which favours e^-/h^+ pair separation. This would also explain the fact that the F-SA has similar rate constants to the P25 with all the substrates studied. This may indicate that the electrostatic effect of the fluoride ion on the anatase phase of the F-SA provokes a similar decrease in the recombination rate of the e^-/h^+ pair to that provoked by the rutile phase in the P25.

4. Conclusions

The synthesis method for the fluorinated materials used in this study (F-P25 and F-SA) generated new catalysts with different properties to those described in other works. The characterisation studies performed with the F-P25 and F-SA catalysts reveal a practically identical surface area and band gap. Small differences are observed in mean particle size between the SA and F-SA and in the anatase/rutile proportions between the P25 and F-P25 which are attributable to the catalyst filtration process. The presence was also seen in the F-P25 and F-SA of isolated hydroxyl groups in a higher relative proportion (in relation to the non-fluorinated catalysts), the absence of Lewis acid sites where the NH_3 is adsorbed and the presence of Brönsted acid sites. It was also determined that interaction of Ti with fluorine atoms generates surface electron traps which cause a baseline increase in the FTIR spectra.

In the studies performed with formic acid, aniline, phenol and phenol-muconic acid mixtures, the k_{formic} , k_{aniline} , and k_{phenol} of the fluorinated catalysts are higher than those of the P25 and SA. With molecules whose adsorption on the catalyst surface is limited, as is the case of phenol and aniline, and whose degradation can take place at the surface/solution interface, the F-P25 and F-SA catalysts generate similar increases in the k_{phenol} with respect to the P25 and SA, respectively. The intermediates identified in phenol degradation suggest that in the fluorinated catalysts the formation of $\bullet\text{OH}_{\text{free}}$ is not favoured. The results obtained indicate that the F-P25

Fig. 12. TOC evolution no corresponding to phenol, hydroquinone, catechol, resorcinol or muconic acid during phenol degradation (A), mixtures phenol: muconic acid 0.51 mM:0.51 mM (B) and mixtures phenol:muconic acid 0.25 mM:0.25 mM (C).

not that of hydroquinone or catechol would suggest that, in the presence of muconic acid, phenol does not have access to the holes

and F-SA promote at the same intensity the sites responsible for the formation of $\bullet\text{OH}_{\text{surf}}$ and surface h^+ .

In this way, it was determined that the fluoride adsorbed on the surface of the F-P25 and F-SA catalysts generates electrostatic fields which favour the reactions of $\bullet\text{OH}_{\text{surf}}$ and h^+ with adsorbed molecules or at the surface/solution interface.

These new catalysts could be promising for processes in gas phase in which the intervention of $\bullet\text{OH}_{\text{surf}}$ and h^+ radicals is a determining factor.

Acknowledgements

We are grateful for the financial support of the Spanish Ministry of Economy and Competitiveness through the projects CTQ2015-64664-C2-1-P and the Spanish Ministry of Science and Innovation for the UNLP10-3E-726 infrastructure, co-financed with ERDF funds. D. Garzón Sousa would like to thank the University of La Palmas de Gran Canaria for its funding through its PhD Grant Program and Wiâm El-Alami would also like to thank the UNetBA Erasmus Program for its funding through a mobility grant.

References

- [1] J. Low, B. Cheng, J. Yu, Surface modification and enhanced photocatalytic CO_2 reduction performance of TiO_2 : a review, *Appl. Surf. Sci.* 392 (2017) 658–686.
- [2] E.M. Samsudin, S.B. Abd Hamid, Effect of band gap engineering in anionic-doped TiO_2 photocatalyst, *Appl. Surf. Sci.* 391 (2017) 326–336.
- [3] E.M. Samsudin, S.B. Abd Hamid, J. Ching Juan, W.J. Basirun, G. Centib, Synergetic effects in novel hydrogenated F-doped TiO_2 photocatalysts, *Appl. Surf. Sci.* 370 (2016) 380–393.
- [4] E.M. Samsudina, S.B. Abd Hamida, J. Ching Juana, W.J. Basiruna, A.E. Kandjanib, S.K. Bhargavaba, Effective role of trifluoroacetic acid (TFA) to enhance the photocatalytic activity of F-doped TiO_2 prepared by modified sol-gel method, *Appl. Surf. Sci.* 365 (2016) 57–68.
- [5] A.A. Sadvonnikov, A.E. Baranchikov, Y.V. Zubavichus, O.S. Ivanova, V.Y. Murzin, V.V. Kozik, V.K. Ivanov, Photocatalytically active fluorinated nano-titania synthesized by microwave-assisted hydrothermal treatment, *J. Photochem. Photobiol. A: Chem.* 303–304 (2015) 36–43.
- [6] C. Minero, G. Mariella, V. Maurino, E. Pelizzetti, Photocatalytic transformation of organic compounds in the presence of inorganic anions. 1. Hydroxyl-mediated and direct electron-transfer reactions of phenol on a titanium dioxide-fluoride system, *Langmuir* 16 (2000) 2632–2641.
- [7] D. Vione, C. Minero, V. Maurino, M.E. Carloti, T. Picatotto, E. Pelizzetti, Degradation of phenol and benzoic acid in the presence of a TiO_2 -based heterogeneous photocatalyst, *Appl. Catal. B: Environ.* 58 (2005) 79–88.
- [8] Y.-C. Oh, W.S. Jenks, Photocatalytic degradation of a cyanuric acid, a recalcitrant species, *J. Photochem. Photobiol. A* 162 (2004) 323–328.
- [9] S. Kim, H. Park, W. Choi, Effects of TiO_2 surface fluorination on photocatalytic reactions and photoelectrochemical behaviors, *J. Phys. Chem. B* 108 (2004) 6402–6411.
- [10] M. Konstantakou, T. Stergiopoulos, V. Likodimos, G.C. Vougioukalakis, L. Sygellou, A.G. Kontos, A. Tserpi, P. Falaras, Influence of fluorine plasma treatment of TiO_2 films on the behavior of dye solar cells employing the Co(II)/(III) redox couple, *J. Phys. Chem. C* 118 (2014) 16760–16775.
- [11] K. Lv, Y. Xu, Effects of polyoxometalate and fluoride on adsorption and photocatalytic degradation of organic dye X3B on TiO_2 : the difference in the production of reactive species, *J. Phys. Chem. B* 110 (2006) 6204–6212.
- [12] J.H. Pan, Z. Cai, Y. Yu, X.S. Zhao, Controllable synthesis of mesoporous F- TiO_2 spheres for effective photocatalysis, *J. Mater. Chem.* 21 (2011) 11430–11438.
- [13] J. Yu, Q. Xiang, J. Ran, S. Mann, One-step hydrothermal fabrication and photocatalytic activity of surface-fluorinated TiO_2 hollow microspheres and tabular anatase single micro-crystals with high-energy facets, *CrystEngComm* 12 (2010) 872–879.
- [14] J. Yu, W. Wang, B. Cheng, B.-L. Su, Enhancement of photocatalytic activity of mesoporous TiO_2 powders by hydrothermal surface fluorination treatment, *J. Phys. Chem. C* 113 (2009) 6743–6750.
- [15] X.F. Cheng, W.H. Leng, D.P. Liu, Y.M. Xu, J.Q. Zhang, C.N. Cao, Electrochemical preparation and characterization of surface-fluorinated TiO_2 nanoporous film and its enhanced photoelectrochemical and photocatalytic properties, *J. Phys. Chem. C* 112 (2008) 8725–8734.
- [16] J. Biedrzycki, E. Livraghi, E. Giamello, S. Agnoli, G. Granozzi, Fluorine- and niobium-doped TiO_2 : chemical and spectroscopic properties of polycrystalline n-type-doped anatase, *J. Phys. Chem. C* 118 (2014) 8462–8473.
- [17] A.M. Czoska, S. Livraghi, M. Chiesa, E. Giamello, S. Agnoli, G. Granozzi, E. Finazzi, C. Di Valentini, G. Pacchioni, The nature of defects in fluorine-doped TiO_2 , *J. Phys. Chem. C* 112 (2008) 8951–8956.
- [18] C. Di Valentini, G. Pacchioni, A. Selloni, Reduced and n-type doped TiO_2 : nature of Ti^{3+} species, *J. Phys. Chem. C* 113 (2009) 20543–20552.
- [19] W.W. Dunn, Y. Aikawa, A.J. Bard, Characterization of particulate titanium dioxide photocatalysts by photoelectroretic and electrochemical measurements, *J. Am. Chem. Soc.* 103 (1981) 3456–3459.
- [20] Y. Xu, K. Lv, Z. Xiong, W. Leng, W. Du, D. Liu, X. Xue, Rate enhancement and rate inhibition of phenol degradation over irradiated anatase and rutile TiO_2 on the addition of NaF: new insight into the mechanism, *J. Phys. Chem. C* 111 (2007) 19024–19032.
- [21] H. Park, W. Choi, Effects of TiO_2 surface fluorination on photocatalytic reactions, *J. Phys. Chem. B* 108 (2004) 4086–4093.
- [22] M. Lewandowski, D.F. Ollis, Halide acid pretreatments of photocatalysts for oxidation of aromatic air contaminants: rate enhancement, rate inhibition, and a thermodynamic rationale, *J. Catal.* 217 (2003) 38–46.
- [23] Q. Xiang, J. Yu, P.K. Wong, Quantitative characterization of hydroxyl radicals produced by various photocatalysts, *J. Colloid Interface Sci.* 357 (2011) 163–167.
- [24] K. Ishibashi, A. Fujishima, T. Watanabe, K. Hashimoto, Detection of active oxidative species in TiO_2 photocatalysis using the fluorescence technique, *Electrochem. Commun.* 2 (2000) 207–210.
- [25] J. Araújo, A. Peña Alonso, J.M. Doña Rodríguez, J.A. Herrera Melián, O. González Díaz, J. Pérez Peña, Comparative study of MTBE photocatalytic degradation with TiO_2 and Cu- TiO_2 , *Appl. Catal. B: Environ.* 78 (2008) 355–363.
- [26] J. Tang, H. Quan, J. Ye, Photocatalytic properties and photoinduced hydrophilicity of surface-fluorinated TiO_2 , *Chem. Mater.* 19 (2007) 116–122.
- [27] D. Li, H. Haneda, S. Hishita, N. Ohashi, N.K. Labhsetwar, Fluorine-doped TiO_2 powders prepared by spray pyrolysis and their improved photocatalytic activity for decomposition of gas-phase acetaldehyde, *J. Fluor. Chem.* 126 (2005) 69–77.
- [28] M. Shariq Vohra, S. Kim, W. Choi, Effects of surface fluorination of TiO_2 on the photocatalytic degradation of tetramethylammonium, *J. Photochem. Photobiol. A: Chem.* 160 (2003) 55–60.
- [29] S. Liu, J. Yu, B. Cheng, M. Jaroniec, Fluorinated semiconductor photocatalysts: tunable synthesis and unique properties, *Adv. Colloid Interface Sci.* 173 (2012) 35–53.
- [30] B. Bahrami, V.G. Komvokis, U.G. Singh, M.S. Ziebarth, O.S. Alexeev, M.D. Amiridis, In situ FTIR characterization of NH_3 adsorption and reaction with O_2 and CO on Pd-based FCC emission control additives, *Appl. Catal. A: Gen.* 391 (2011) 11–21.
- [31] A.C. Sola, D. Garzón Sousa, J. Araújo, O. González Díaz, J.M. Doña Rodríguez, P. Ramírez de la Piscina, N. Homs, Differences in the vapour phase photocatalytic degradation of ammonia and ethanol in the presence of water as a function of TiO_2 characteristics and the presence of O_2 , *Catal. Today* 266 (2016) 53–61.
- [32] K. Hadjiivanov, H. Knözinger, Species formed after NO adsorption and $\text{NO} + \text{O}_2$ co-adsorption on TiO_2 : an FTIR spectroscopic study, *Phys. Chem. Chem. Phys.* 2 (2000) 2803–2806.
- [33] P. Pagsberg, B. Sztube, E. Ratajczak, A. Sillesen, Spectrokinetic studies of the gas phase reactions $\text{NH}_2 + \text{NO}_x$ initiated by pulse radiolysis, *Acta Chem. Scand.* 45 (1991) 329–334.
- [34] X. Zhang, Q.S. Li, Direct dynamics study on the reaction of N_2H_4 with F atom: a hydrogen abstraction reaction? *J. Phys. Chem. A* 110 (2006) 11636–11644.
- [35] K. Lv, X. Guo, X. Wu, Q. Li, W. Ho, M. Li, H. Ye, D. Du, Photocatalytic selective oxidation of phenol to produced hydroxy benzenes in a TiO_2/UV system: hydroxyl radical versus hole, *Appl. Catal. B* 199 (2016) 405–411.
- [36] H. Sheng, Q. Li, W. Ma, H. Ji, C. Chen, J. Zhao, Photocatalytic degradation of organic pollutants on surface anionized TiO_2 : common effect of anions for high hole-availability by water, *Appl. Catal. B: Environ.* 138–139 (2013) 212–218.
- [37] J. Araújo, E. Pulido Melián, V.M. Rodríguez López, A. Peña Alonso, J.M. Doña Rodríguez, O. González Díaz, J. Pérez Peña, Photocatalytic degradation of phenol and phenolic compounds Part I. Adsorption and FTIR study, *J. Hazard. Mater.* 146 (2007) 520–528.
- [38] M. Canle L, J.A. Santaballa, E. Vulliet, On the mechanism of TiO_2 -photocatalyzed degradation of aniline derivatives, *J. Photochem. Photobiol. A* 175 (2005) 192–200.
- [39] M.F.J. Dijkstra, H.J. Panneman, J.G.M. Winkelman, J.J. Kelly, A.A.C.M. Beenackers, Modeling the photocatalytic degradation of formic acid in a reactor with immobilized catalyst, *Chem. Eng. Sci.* 57 (2002) 4895–4907.
- [40] X. Ma, Y. Dai, M. Guo, B. Huang, Relative photooxidation and photoreduction activities of the {100}, {101}, and {001} surfaces of anatase TiO_2 , *Langmuir* 29 (2013) 13647–13654.
- [41] B. Sun, Alexandre V. Vorontsov, P.G. Smirniotis, Role of platinum deposited on TiO_2 in phenol photocatalytic oxidation, *Langmuir* 19 (2003) 3151–3315.
- [42] N. Watanabe, S. Horikoshi, H. Hidaka, N. Serpone, On the recalcitrant nature of the triazinic ring species cyanuric acid, to degradation in Fenton solutions and in UV-illuminated TiO_2 (naked) and fluorinated TiO_2 aqueous dispersions, *J. Photochem. Photobiol. A: Chem.* 174 (2005) 229–238.
- [43] C. Minero, G. Mariella, V. Maurino, D. Vione, E. Pelizzetti, Photocatalytic transformation of organic compounds in the presence of inorganic ions 2. Competitive reactions of phenol and alcohols on a titanium dioxide-fluoride system, *Langmuir* 16 (2000) 8964–8972.